Talanta 112 (2013) 31–36

Contents lists available at SciVerse ScienceDirect

Talanta

journal homepage: www.elsevier.com/locate/talanta

Selective and sensitive determination of uric acid in the presence of ascorbic acid and dopamine by PDDA functionalized graphene/graphite composite electrode

Yanyan Yu [a], Zuanguang Chen [a,*], Beibei Zhang [a], Xinchun Li [b], Jianbin Pan [a]

[a] School of Pharmaceutical Sciences, Sun Yat-sen University, Guangzhou 510006, China
[b] School of Pharmaceutical Sciences, Guangxi Medical University, Nanning 530021, China

ARTICLE INFO

Article history:
Received 12 December 2012
Received in revised form
16 March 2013
Accepted 23 March 2013
Available online 29 March 2013

Keywords:
Graphene
Poly(diallyldimethylammonium chloride)
Uric acid
Modified electrode
Biosensor

ABSTRACT

In this work, a facile electrochemical sensor based on poly(diallyldimethylammonium chloride) (PDDA) functionalized graphene (PDDA-G) and graphite was fabricated. The composite electrode exhibited excellent selectivity and sensitivity towards uric acid (UA), owing to the electrocatalytic effect of graphene nanosheets and the electrostatic attractions between PDDA-G and UA. The anodic peak current of UA obtained by cyclic voltammetry (CV) increased over 10-fold compared with bare carbon paste electrode (CPE). And the reversibility of the oxidation process was improved significantly. Differential pulse voltammetry (DPV) was used to determine UA in the presence of ascorbic acid (AA) and dopamine (DA). It was found that all of oxidation peaks of three species could be well resolved, and the peak current of UA was much stronger than the other two components. More importantly, considerable-amount of AA and DA showed negligible interference to UA assay. The calibration curve for UA ranged from 0.5 to 20 μmol L^{-1} with a correlation coefficient of 0.9934. The constructed sensor has been employed to quantitatively determine UA in urine samples.

1. Introduction

Graphene, a two-dimensional sheet of sp^2 bonded carbon atoms perfectly arranged in a honeycomb lattice [1], has received significant attention. Due to its unique physicochemical properties [2], graphene has already demonstrated enormous potentials in a variety of fields [3–5]. Several methods have been presented to synthesize graphene, including chemical vapor deposition (CVD) [6], plasma enhanced chemical vapor deposition [7], solvothermal method [8], exfoliation and cleavage of natural graphite [9], and so on [10–12]. Among them, chemical reduction of graphene oxide (GO) is considered to be the most common and economical method [13]. However, during the chemical conversion course, graphene nanosheets are apt to aggregate [14]. Therefore, graphene-modified materials (e.g. polyelectrolyte and surfactant) through noncovalent or covalent bonding have become a focus of research. Compared to covalent methods, noncovalent strategies are attracting more and more attention as they allow for enhanced solubility, and superior electrochemical properties [15]. Polyaniline [16], 1-pyrenebutyrate [17], cyclodextrin [18], single-stranded DNA [19] and protein [20] have been utilized to stabilize graphene sheets.

Poly(diallyldimethylammonium chloride), PDDA, not only an electronic conducting polymer but also a strong ionic polymer [21], has been extensively used combining with other materials, such as multi-walled carbon nanotubes (MWCNTs) [22] and metal nanoparticles [23] to modify electrodes. Recently, PDDA has been reported to exhibit excellent binding capability with graphene nanosheets [24–26]. Luo et al. [27] reported that PDDA functionalized graphene (PDDA-G) showed good conductivity, solubility and biocompatibility. PDDA-G has also been proved to exhibit electrocatalytic activity for oxygen reduction [28], catechol and hydroquinone oxidation [29]. Therefore, PDDA-G has great potential to fabricate chemically modified electrode.

Uric acid (UA, 12,6,8-trihydroxypurine), is the end product of catabolism of the purine nucleosides. Elevated level of uric acid in the blood is clinically pertinent to gout, renal failure, leukemia and lymphoma, as well as other pathological conditions [30]. Numerous analytical approaches including chemiluminescence, chromatography, enzymatic methods and so forth [31,32] have been reported for the quantitation of UA. Electrochemical techniques have been frequently applied for the determination of UA in a variety of biological matrixes [30,33,34]. Whereas, direct electrochemistry of UA at bare solid electrodes requires high overpotentials and suffers from interferences from other substances

* Corresponding author. Tel.: +86 20 3994 3044; fax: +86 20 3994 3071.
E-mail address: chenzg@mail.sysu.edu.cn (Z. Chen).

0039-9140/$ - see front matter © 2013 Elsevier B.V. All rights reserved.
http://dx.doi.org/10.1016/j.talanta.2013.03.057

coexisting in biological fluids, such as ascorbic acid (AA) and dopamine (DA), whose oxidation potentials are very close to that of UA, resulting in poor selectivity and reproducibility [35]. Up to now, modified electrodes have been overwhelmingly employed to improve the selectivity for the detection of UA, such as metal complex and nanoparticles [36,37], enzymes [31,38], polymers [35,39] and carbon-based materials [30]. Although, these methods reported have some advantages (low limit of detection and favorable selectivity), tedious preparation and instability of electrodes still remain intractable. There still exist expanding demands for the development of facile, rapid and specific electrochemical sensors for UA.

Herein, we presented, for the first time, a PDDA-G modified carbon paste electrode (PDDA-G/CPE). The electrode was facile to fabricate and showed excellent electrochemical properties. Cyclic voltammetry (CV) and differential pulse voltammetry (DPV) were used to evaluate the electrochemical behavior of UA at the prepared composite electrode. A rapid and sensitive response towards UA oxidation was exhibited by the modified sensor. As for the measurement of UA in the presence of AA and DA, remarkably enhanced electrochemical response was obtained and the oxidation peak of UA can be well separated with the other substances at the modified electrode. The present work paves a way towards broadening the applications of graphene in electrochemical biosensors.

2. Experiments

2.1. Material, chemicals and reagents

All chemicals were used as received unless otherwise stated. Graphite oxide was obtained from Nanjing XF NANO Materials Tech Co., Ltd (Nanjing China). Sodium phosphate monobasic, sodium phosphate dibasic, nitric acid, sodium hydroxide and liquid paraffin were obtained from Sinopharm reagent (Shanghai, China). UA, AA, dopamine hydrochloride, hydrazine hydrate and PDDA (MW=200,000–350,000, 20 wt% in water) were from Aladin Chemistry Co. Ltd (Shanghai, China). Fused silica capillary (150 μm I.D., 360 μm O.D.) used for electrodes fabrication was from Refine Chromatographics (Hebei, China). Phosphate buffer solutions (PBS, 0.1 mol L^{-1}) were prepared by mixing the stock solutions of 0.2 mol L^{-1} NaH_2PO_4 and Na_2HPO_4. Stock solution of UA was prepared daily in 5 mM NaOH aqueous solution. Stock solutions of AA and DA were made daily in redistilled water. All stock solutions were diluted with supporting electrolyte to desired concentrations for analysis.

2.2. Apparatus and measurements

CV and DPV were performed on an electrochemical analyzer (μ-EA160C), which was provided by South China University of Technology (Guangzhou, China). A conventional three-electrode system was employed. An Ag/AgCl (saturated KCl) electrode and a platinum wire electrode were used as reference electrode and counter electrode, respectively. Bare or modified carbon paste electrode was used as working electrode. All the electrochemical measurements were operated in ambient conditions. FT-IR spectra were recorded on a TENSOR37 spectrometer (Bruker). UV–vis absorption spectra were obtained using a UV2450 spectrophotometer (Shimadzu). The Raman spectra were carried out using Renishaw inVia laser micro-Raman spectrometer. Scanning electron microscopy (SEM) images were obtained from Quanta 400F thermal field emission environmental SEM (FEI).

2.3. Synthesis of PDDA-G

PDDA-G was obtained by reduction of GO in the presence of PDDA. GO aqueous dispersion was obtained from graphite oxide by sonication and centrifugation. 100 mL of GO (0.5 mg mL^{-1}) was loaded in a 250-mL round-bottom flask, followed by the addition of 500 μL PDDA (20 wt%) to form an inhomogeneous yellow-brown dispersion. This dispersion was sonicated until there was no visible particulate, then it was kept stirring for 2 h. Thereafter, 50 μL of hydrazine hydrate was added. After being vigorously shaken or stirred for a few minutes, the flask was put in an oil bath at 95 °C equipped with a water-cooling condenser for 1 h to produce a homogeneous black suspension. The final product (PDDA-G) was collected through centrifugation and dried by freeze-drying. To obtain the unfunctionalized graphene, the above procedure was adopted just in the absence of PDDA.

2.4. Electrode fabrication and modification

Graphite powder (0.1 g) was mixed with varying amounts of the processed PDDA-G using liquid paraffin in an agate mortar. After thorough grinding, a homogeneous paste was obtained. The resulting paste was pressed into a portion of silica capillary to a depth of ~3 mm. Finally, the paste electrode was polished on a piece of weighing paper to get a flat surface. For comparison, graphene modified electrode (G/CPE) and GO modified electrode (GO/CPE) were constructed in the similar manner described above. All the electrodes were stored at 4 °C when not in use.

3. Results and discussion

3.1. Characterizations

Fig. 1A displayed the SEM image of PDDA-G. Clearly, there were some corrugations and scrolling of the nanosheets. Meanwhile, there were some aggregations of the nanosheets. UV–vis and FT-IR spectroscopy were utilized to monitor the reduction of GO and concomitant functionalization process. As shown in Fig. 1B, the UV–vis spectrum of GO dispersion exhibited a strong band at 225 nm. As for the PDDA-G, the absorption peak red shifted to 264 nm and the absorption in the whole spectral region increased significantly in comparison with GO. This phenomenon suggested that GO was reduced and the electronic conjugation within the graphene sheets was restored upon hydrazine reduction. Moreover, the reduction process was accompanied by an obvious color change from yellow–brown (GO) to black (PDDA-G), as shown in the inset photograph. We can see from Fig. 1C that the FT-IR spectrum of GO showed a strong absorption peak around 1724 cm^{-1}, attributed to the skeletal vibration of C=O. The spectrum also showed other characteristic peaks, namely, O–H (3369 and 1404 cm^{-1}), C=C (1624 cm^{-1}), and C=O (1055 cm^{-1}). The reduction of GO to graphene was evidenced by the obvious decrease in absorption bands of oxide groups (C=O, O–H, C–O). Fig. 1C also suggested that adsorption of PDDA did not make much difference to the reduction of GO, as the oxide groups were all well reduced. Meanwhile, the appearance of new peak around 1467 cm^{-1} was attributable to the N–C bond in the adsorbed PDDA.

Raman spectroscopy was a powerful technique to determine the defects and the layers of graphene. As known, D peak was associated with structural defects due to intervalley scattering and G referred to the graphene G peak [40]. As illustrated in Fig. 1D, GO displayed two prominent peaks at ~1602 and ~1346 cm^{-1} corresponding to the G and D peaks, respectively. The spectrum of PDDA-G also contained both G and D peaks at 1595 and

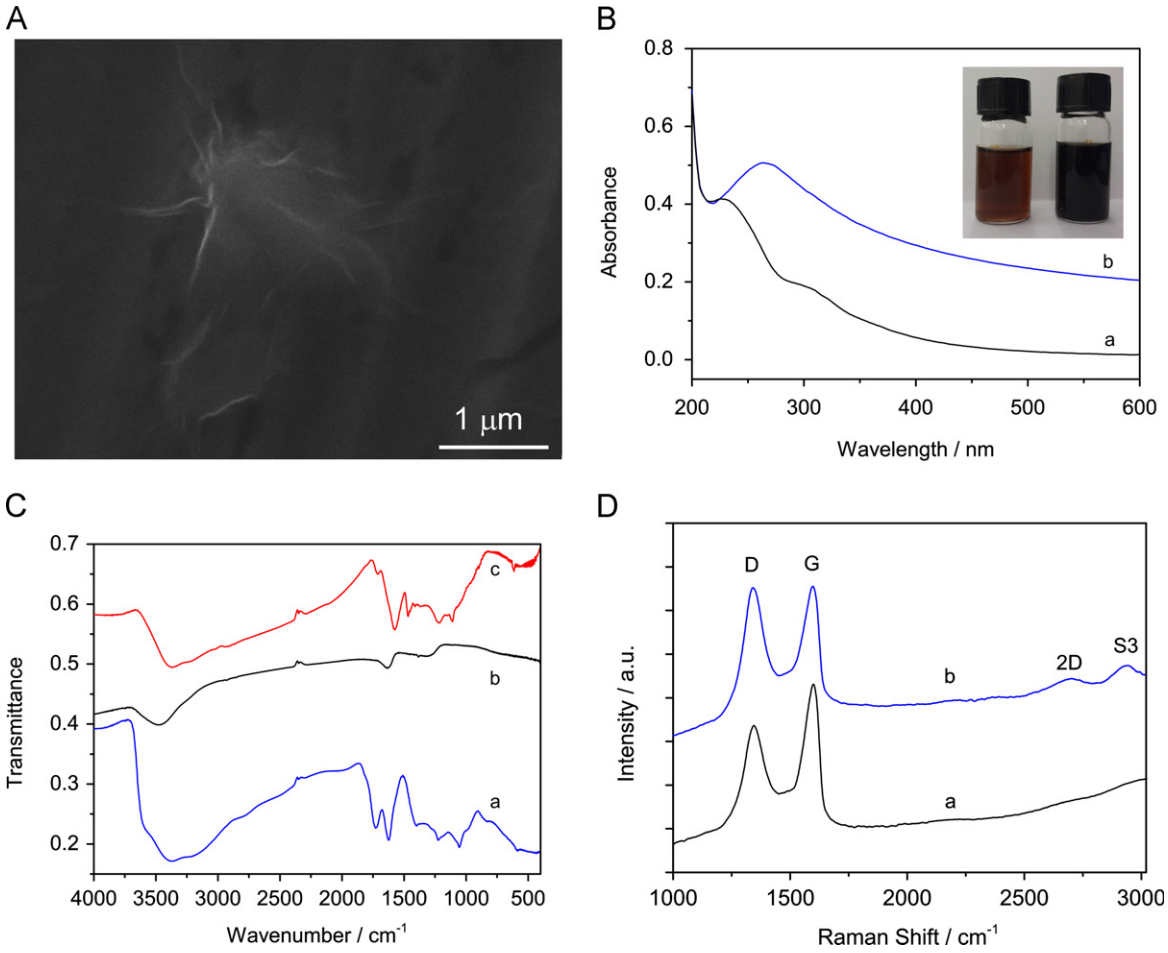

Fig. 1. (A) SEM image of PDDA-G. (B) UV–vis absorption spectra of GO (a) and PDDA-G (b). Inset: the photograph of aqueous dispersion of GO (left) and PDDA-G (right). (C) FT-IR spectra of GO (a), graphene (b), and PDDA-G (c). (D) Raman spectra of GO (a) and PDDA-G (b). (For interpretation of the references to color in this figure legend, the reader is referred to the web version of this article.)

1344 cm^{-1}. The D/G intensity ratio increased notably from GO to PDDA-G, suggesting an increase in the number of smaller graphene domains after reduction. The intensity of the 2D (~2708 cm^{-1}) and S3 (~2948 cm^{-1}) peaks of PDDA-G, where 2D was the graphene 2D peak, and S3 peak referred to a second-order peak due to the D–G combination, also increased compared with that of GO, showing better graphitization.

3.2. Effect of the proportion of PDDA-G on the performance of PDDA-G/CPE

Adsorption of PDDA onto the graphene sheets can create net positive charge on carbon atoms in the all-carbon graphene plane via the intermolecular charge transfer [28], thus facilitating the interaction with negatively charged UA molecules through electrostatic attracting interaction. Meanwhile, with excellent electron-transfer ability, graphene can also promote the oxidation of UA. Consequently, the amount of PDDA-G is accordingly an essential consideration when fabricating the UA sensor. Fig. 2 depicted that the CV responses of 1 mmol L^{-1} UA in 0.1 mol L^{-1} PBS altered with the variation of the mass proportion of PDDA-G in the electrode. Oxidation peak currents enhanced with the increasing proportion of PDDA-G, and finally reached a platform at amount of 30%. On the other hand, the oxidation peak potential shifted negatively in the same condition and reached its minimum at the same point. As higher proportion of PDDA-G would result in higher charging currents, 30% was chosen thereafter for the electrode fabrication.

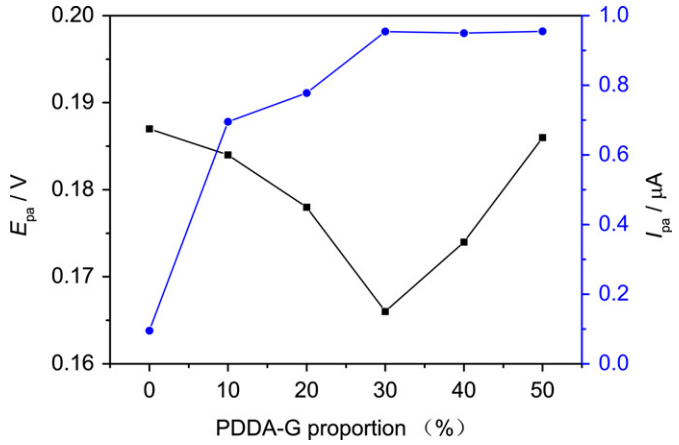

Fig. 2. Influence of PDDA-G proportion in the sensor on peak potential (diamond) and oxidation peak current (circle) of 1 mmol L^{-1} UA in 0.1 mol L^{-1} PBS (pH 7.0) at a scan rate of 50 mV s^{-1}.

3.3. Electrochemical behaviors of UA at the modified electrodes

We also investigated the electrocatalytic ability of the prepared sensor by determining UA in 0.1 mol L^{-1} PBS (pH 7.0) with a scan rate of 50 mV s^{-1}. Cyclic voltammograms of 1 mmol L^{-1} UA at different electrodes were comparatively illustrated in Fig. 3. The electrocatalytic oxidation of UA by PDDA-G was evidenced by the significant increase of the oxidation peak current, 10-fold higher

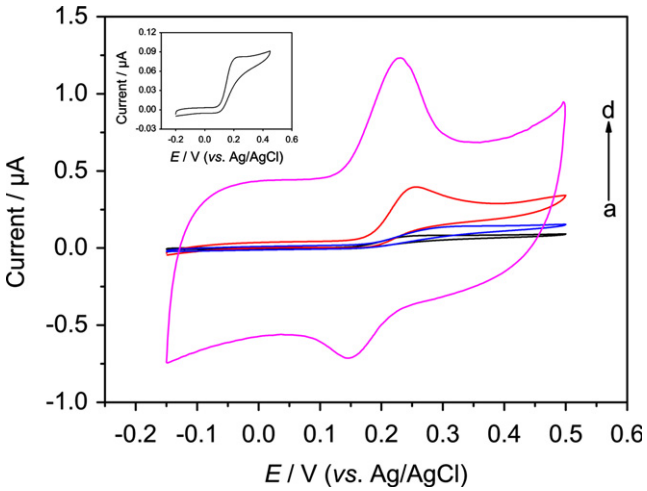

Fig. 3. Cyclic voltammograms of 1 mmol L^{-1} UA at CPE (a), G/CPE (b), GO/CPE (c) and PDDA-G/CPE (d) in 0.1 mol L^{-1} PBS (pH 7.0) with a scan rate of 50 mV s^{-1}. Inset: Cyclic voltammograms of 1 mmol L^{-1} UA at CPE.

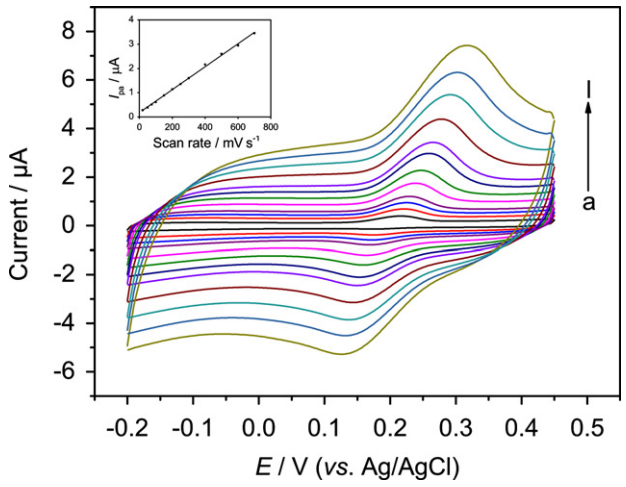

Fig. 4. Cyclic voltammograms of 1 mmol L^{-1} UA at the PDDA-G/CPE at different scan rates (a-l: 20, 50, 75, 100,150, 200, 250, 300, 400, 500, 600 and 700 mV s^{-1}) in 0.1 mol L^{-1} PBS (pH 7.0). Inset: the plot of the oxidation peak currents versus scan rates.

compared with bare CPE. G/CPE, however, showed little increased response than the bare CPE, as graphene nanosheets aggregated severely during the drying procedure resulting in a great loss of electrocatalytic effect [2]. Therefore, it was reasonable to claim that PDDA played a vital role in the electrocatalytic effect of graphene. The illustration also suggested that the electrocatalytic behavior of GO was arrestive [41], whereas the catalytic current was much lower than that at PDDA-G/CPE. On the other hand, there was only an oxidation peak for UA at bare CPE, which indicated that the oxidation process was irreversible and the electro-transfer kinetics were slow. By contrast, UA gave a pair of redox peaks at PDDA-G/CPE, suggesting a highly improved reversibility of the reaction process. The enhancement of the current as well as the improvement of the reversibility confirmed that the electrocatalytic effect of graphene was remarkably enhanced by the adsorption of PDDA.

3.4. Effect of scan rate on the electrochemical performance of PDDA-G/CPE

CV was utilized to investigate the effect of scan rate on the redox reaction of UA at the PDDA-G/CPE in 0.1 mol L^{-1} PBS (pH 7.0) with scan rates ranging from 20 to 700 mV s^{-1}. As shown in Fig. 4, the oxidation peak currents were linearly related with the scan rates. The linear regression equation was I_{pa} (μA)=0.1796 +0.00473ν (mV s^{-1}), with a correlation coefficient 0.9992. It was worth noting that the reduction peak currents also increased linearly with the scan rates but not so sharply as in the case of the oxidation process. With increasing the scan rate, the oxidation peak potential shifted positively and the reduction peak potential shifted negatively. All these characteristics suggested that the redox reaction of UA at the PDDA-G/CPE was a predominantly surface-controlled electrochemical process.

3.5. Amperometric response of UA at the PDDA-G/CPE

The amperometric response of PDDA-G/CPE at a constant potential of 0.4 V upon successive addition of UA into supporting electrolyte (0.1 mol L^{-1} PBS, pH 7.0) was illustrated in Fig. 5. Obviously, the heights of current steps were proportional to the concentrations of UA added into the stirring solution. A clear current step could be observed upon addition of 0.5 μmol L^{-1} UA, suggesting high sensitivity of the electrode. The oxidation currents achieved 95% of the steady-state current within 4 s, revealing a

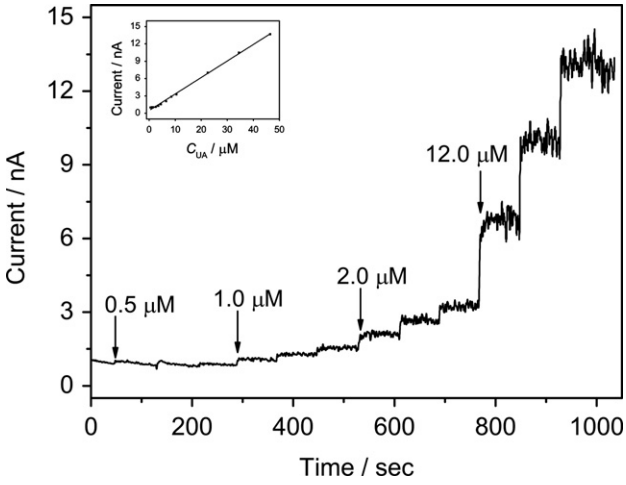

Fig. 5. Amperometric response of PDDA-G/CPE at a constant potential of 0.4 V upon successive addition of UA solution into 0.1 mol L^{-1} PBS (pH 7.0). Inset: the linear relationship of steady-state currents versus UA concentrations.

rapid response of the electrochemical sensor. The plot of inset depicted a linear relationship between the steady-state currents and concentrations of UA. The linear regression equation was defined as I (nA)=0.4741+0.2856C_{UA} (μmol L^{-1}), with a correlation coefficient of 0.9973.

3.6. Determination of UA in the presence of abundant AA and DA

As mentioned above, DA and AA always coexist with UA in biological fluids. The oxidation potentials of these three species are always close, thus overlap of the oxidation peaks and interferences from the other two species are major problems encountered in UA detection. Therefore, the interferences from AA and DA were investigated by CV and DPV. Fig. 6A depicted the cyclic voltammograms obtained from a ternary mixture containing 1 mmol L^{-1} AA, 1 mmol L^{-1} DA, and 0.1 mmol L^{-1} UA at different electrodes. Obviously, the voltammetric responses of the three elements were separated successfully on the PDDA-G/CPE with well-defined peaks and remarkably enhanced peak currents. The responses at the bare CPE, G/CPE and GO/CPE were overlapped weak peaks, indicating the poor selectivity and sensitivity.

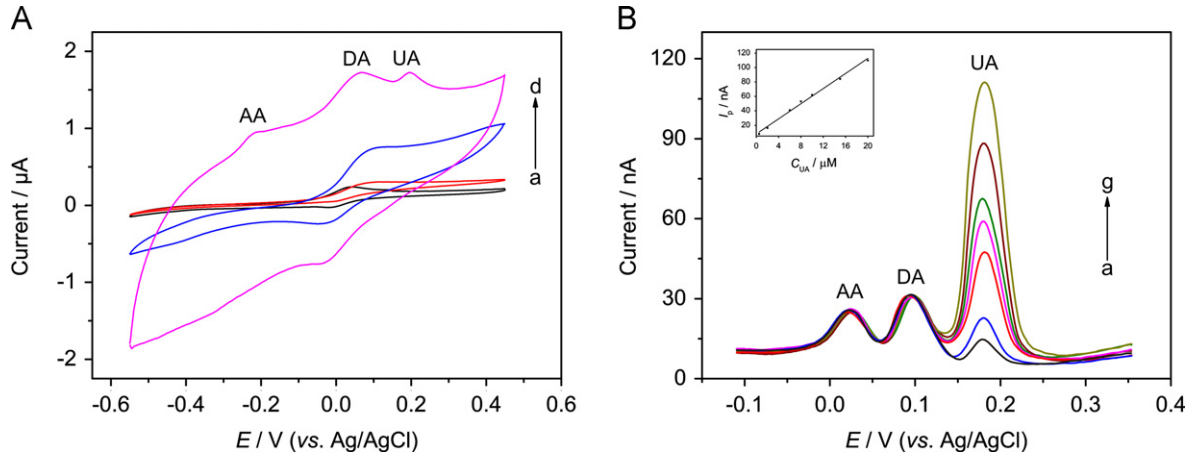

Fig. 6. (A) Cyclic voltammograms of 1 mmol L^{-1} AA, 1 mmol L^{-1} DA, and 0.1 mmol L^{-1} UA at CPE (a), G/CPE (b), GO/CPE (c) and PDDA-G/CPE (d) in 0.1 mol L^{-1} PBS (pH 7.0) with a scan rate of 50 mV s^{-1}. (B) Differential pulse voltammograms of (a–g) 0.5, 2, 6, 8, 10, 15, 20 μmol L^{-1} UA in the presence of 100 μmol L^{-1} AA and 100 μmol L^{-1} DA at PDDA-G/CPE in 0.1 mol L^{-1} PBS (pH 7.0). Inset: linear relationship of peak currents versus UA concentrations. The parameters of DPV: amplitude, 50 mV; pulse width, 0.05 s; pulse period, 0.2 s.

DPV was further carried out to assess the interferences from AA and DA at PDDA-G/CPE. During the procedure, the concentration of UA varied, whereas AA and DA remained constant. Fig. 6B showed the differential pulse voltammograms of 100 μmol L^{-1} AA, 100 μmol L^{-1} DA and various concentrations of UA in 0.1 mol L^{-1} PBS (pH 7.0). Three well-resolved peaks could be observed, with oxidation peak potentials of 0.025 V for AA, 0.097 V for DA and 0.18 V for UA. When the concentration of UA varied, the peak currents of AA and DA remained constant, demonstrating the independent responses of the three species. Comparatively, PDDA-G/CPE exhibited much bigger response for the oxidation of UA than for AA and DA. Meanwhile, there were no interferences observed from high concentrations of the two elements. As reported [42], the oxidation potential of DA was really close to UA and the electrochemical response of DA was usually strong, making it a great potential interference for detecting UA. At the PDDA-G/CPE, however, the oxidation process of DA was effectively suppressed. The electrochemical response of UA was about 25 times higher than DA and quantitative detection of UA was achieved even in the presence of 200-fold DA. The high selectivity and sensitivity may be attributed to the positively charged graphene sheets in the composite electrode. As DA was an anion under the oxidation condition, the repulsive force between DA and PDDA-G resulting from electrostatic interactions suppressed the oxidation process. As shown in the inset of Fig. 6B, the oxidation peak currents increased linearly with the concentration of UA ranging from 0.5 to 20 μmol L^{-1}. The linear regression equation was I (nA)=7.990+5.241C_{UA} (μmol L^{-1}) with a correlation coefficient of 0.9934. The limit of detection (LOD, S/N=3) and the capability of detection ($\alpha=\beta=0.05$) were determined to be 0.08 and 0.97 μmol L^{-1}, respectively. Therefore, it was reliable and feasible to selectively determine UA at PDDA-G modified electrode.

3.7. Stability of the PDDA-G/CPE

Further assessment of stability of the electrode was conducted through DPV of 15 μmol L^{-1} UA on consecutive days. The peak currents of UA remained 89.9% initial value after 20 days, indicating the considerable stability of the modified electrode. To evaluate the repeatability (intrasensors) of the electrode, the peak currents of six successive measurements by DPV of 15 μmol L^{-1} UA were detected. And the results showed relative standard deviation (RSD) of 2.1%. As for the reproducibility (intersensors), six electrodes were fabricated to detect UA in the above solution. The RSD of the peak currents was 3.6%. These results showed that the PDDA-G/CPE had good repeatability and acceptable reproducibility for analytical applications.

Table 1
Comparison of analytical performance of PDDA-G/CPE with other modified electrodes in the literature.

Electrode materials	Linear range (μmol L^{-1})	LOD (μmol L^{-1})	Repeatability[f] (RSD%)	Reproducibility[g] (RSD%)	Reference
AuNPs/CPE [a]	6–180	0.71	1.41	–	[43]
Poly(L-Arg)/G/GCE[b]	0.1–10	0.05	2.0	2.2	[44]
5-HTP/GCE[c]	0.5–11	0.28	2.7	–	[45]
BCP/GCE[d]	0.5–120	0.2	1.6	2.2	[46]
Pd/CNFs[e]	2–200	0.7	3.24	3.78	[36]
PDDA-G/CPE	0.5–20	0.08	2.1	3.6	This work

[a] Gold nanoparticles modified carbon paste electrode.
[b] Poly(L-arginine)/graphene composite film modified glassy carbon electrode.
[c] 5-Hydroxytryptophan modified glassy carbon electrode.
[d] Bromocresol purple modified glassy carbon electrode.
[e] Palladium nanoparticle-loaded carbon nanofibers.
[f] Repeatability of intrasensor.
[g] Reproducibility of intersensors.

The comparison of performances of different modified electrodes for UA determination was presented in Table 1. It can be observed that the proposed electrode in the present paper had a comparable performance in UA analysis.

3.8. Real sample analysis

The proposed composite electrode was employed to determine UA in human urine samples. The samples were collected from laboratory co-workers and diluted 500-fold with PBS (pH 7.0) before measurement, aiming to fit the linear range and also to eliminate the matrix effects. No other pretreatment process was performed. To ascertain the accuracy of the results, standard addition method was performed. The analysis data of human urine samples were summarized in Table 2. As shown, the recovery rates of the spiked samples were between 95% and 102.8%. The UA concentration of the samples were determined as 2690, 2835, 2645 μmol L^{-1}, respectively. The results indicated

Table 2
Determination of UA in human urine samples using PDDA-G/CPE.

No.	Detected (μmol L^{-1})	Added (μmol L^{-1})	Found[a] (μmol L^{-1})	RSD (%)	Recovery[a] (%)
1	5.38	1.00	6.34 ± 0.19	2.94	96.0 ± 18.6
		5.00	10.52 ± 0.33	3.12	102.8 ± 6.6
		10.00	15.22 ± 0.43	2.87	98.4 ± 4.3
2	5.67	1.00	6.62 ± 0.23	3.43	95.0 ± 22.7
		6.00	11.55 ± 0.37	3.24	98.0 ± 6.2
		10.00	15.75 ± 0.48	3.05	100.8 ± 4.8
3	5.29	1.00	6.26 ± 0.20	3.27	97.0 ± 20.4
		5.00	10.34 ± 0.32	3.16	101.0 ± 6.4
		10.00	15.21 ± 0.47	3.08	99.2 ± 4.7

[a] Values represented mean $\pm$ SD ($n=3$).

that the method developed was reliable and applicable to determine UA in human urine samples.

4. Conclusions

In this work, a novel CPE modified with PDDA-G was successfully fabricated. The electrochemical sensor exhibited higher selectivity and favorable sensitivity towards the oxidation of UA. Well-separated peaks and enhanced peak currents were obtained by CV and DPV without interference from excess AA and DA, indicating that the PDDA-G facilitated the determination of UA. Additionally, the modified electrode was employed to detect UA in real samples and satisfactory results were obtained. With excellent electrochemical catalytic ability and selectivity, PDDA-G/CPE may attract more attention in the field of electrochemical analysis of biological samples.

Acknowledgements

Financial supports from the National Natural Science Foundation of China (Nos. 20727006, 21075139), the Fundamental Research Funds for the Central Universities, and Guangdong Provincial Science and Technology Project (No. 2008A030102009) are gratefully acknowledged.

References

[1] K.S. Novoselov, A.K. Geim, S.V. Morozov, D. Jiang, Y. Zhang, S.V. Dubonos, I.V. Grigorieva, A.A. Firsov, Science 306 (2004) 666–669.
[2] X. Huang, X.Y. Qi, F. Boey, H. Zhang, Chem. Soc. Rev. 41 (2012) 666–686.
[3] H.X. Tang, G.J. Ehlert, Y.R. Lin, H.A. Sodano, Nano Lett. 12 (2012) 84–90.
[4] P. Verma, P. Novak, Carbon 50 (2012) 2599–2614.
[5] M. Zhou, Y.M. Zhai, S.J. Dong, Anal. Chem. 81 (2009) 5603–5613.
[6] K.S. Kim, Y. Zhao, H. Jang, S.Y. Lee, J.M. Kim, K.S. Kim, J.H. Ahn, P. Kim, J.Y. Choi, B.H. Hong, Nature 457 (2009) 706–710.
[7] Y. Wang, X.F. Xu, J. Lu, M. Lin, Q.L. Bao, B. Ozyilmaz, K.P. Loh, ACS Nano 4 (2010) 6146–6152.
[8] M. Choucair, P. Thordarson, J.A. Stride, Nat. Nanotechnol. 4 (2009) 30–33.
[9] Y. Hernandez, V. Nicolosi, M. Lotya, F.M. Blighe, Z.Y. Sun, S. De, I.T. McGovern, B. Holland, M. Byrne, Y.K. Gun'ko, J.J. Boland, P. Niraj, G. Duesberg, S. Krishnamurthy, R. Goodhue, J. Hutchison, V. Scardaci, A.C. Ferrari, J.N. Coleman, Nat. Nanotechnol. 3 (2008) 563–568.
[10] Z.Y. Lin, Y.G. Yao, Z. Li, Y. Liu, Z. Li, C.P. Wong, J. Phys. Chem. C 114 (2010) 14819–14825.
[11] L.J. Cote, R. Cruz-Silva, J.X. Huang, J. Am. Chem. Soc. 131 (2009) 11027–11032.
[12] I.K. Moon, J. Lee, R.S. Ruoff, H. Lee, Nat. Commun. 1 (2010).
[13] Y.Y. Shao, J. Wang, H. Wu, J. Liu, I.A. Aksay, Y.H. Lin, Electroanalysis 22 (2010) 1027–1036.
[14] X.Y. Qi, K.Y. Pu, H. Li, X.Z. Zhou, S.X. Wu, Q.L. Fan, B. Liu, F. Boey, W. Huang, H. Zhang, Angew. Chem. Int. Ed. 49 (2010) 9426–9429.
[15] X.Y. Qi, K.Y. Pu, X.Z. Zhou, H. Li, B. Liu, F. Boey, W. Huang, H. Zhang, Small 6 (2010) 663–669.
[16] K. Zhang, L.L. Zhang, X.S. Zhao, J.S. Wu, Chem. Mater. 22 (2010) 1392–1401.
[17] Y.X. Xu, H. Bai, G.W. Lu, C. Li, G.Q. Shi, J. Am. Chem. Soc. 130 (2008) 5856.
[18] Y.J. Guo, S.J. Guo, J.T. Ren, Y.M. Zhai, S.J. Dong, E.K. Wang, ACS Nano 4 (2010) 4001–4010.
[19] Q.A. Zhang, Y. Qiao, F. Hao, L. Zhang, S.Y. Wu, Y. Li, J.H. Li, X.M. Song, Chem. Eur. J. 16 (2010) 8133–8139.
[20] J.B. Liu, S.H. Fu, B. Yuan, Y.L. Li, Z.X. Deng, J. Am. Chem. Soc. 132 (2010) 7279 $\pm$.
[21] G. Marcelo, M.P. Tarazona, E. Saiz, Polymer 46 (2005) 2584–2594.
[22] N. Alexeyeva, K. Tammeveski, Anal. Chim. Acta 618 (2008) 140–146.
[23] S.P. Jiang, Z.C. Liu, H.L. Tang, M. Pan, Electrochim. Acta 51 (2006) 5721–5730.
[24] K.P. Liu, J.J. Zhang, G.H. Yang, C.M. Wang, J.J. Zhu, Electrochem. Commun. 12 (2010) 402–405.
[25] X.X. Liu, H. Zhu, X.R. Yang, Talanta 87 (2011) 243–248.
[26] D.B. Lu, Y. Zhang, L.T. Wang, S.X. Lin, C.M. Wang, X.F. Chen, Talanta 88 (2012) 181–186.
[27] B.M. Luo, X.B. Yan, S. Xu, Q.J. Xue, Electrochim. Acta 59 (2012) 429–434.
[28] S. Zhang, Y.Y. Shao, H.G. Liao, M.H. Engelhard, G.P. Yin, Y.H. Lin, ACS Nano 5 (2011) 1785–1791.
[29] L.T. Wang, Y. Zhang, Y.L. Du, D.B. Lu, Y.Z. Zhang, C.M. Wang, J. Solid State Electrochem. 16 (2012) 1323–1331.
[30] J.C. Ndamanisha, L.P. Guo, Biosens. Bioelectron. 23 (2008) 1680–1685.
[31] J. Galban, Y. Andreu, M.J. Almenara, S. de Marcos, J.R. Castillo, Talanta 54 (2001) 847–854.
[32] D. Lakshmi, M.J. Whitcombe, F. Davis, P.S. Sharma, B.B. Prasad, Electroanalysis 23 (2011) 305–320.
[33] J. Wang, M.P. Chatrathi, Anal. Chem. 75 (2003) 525–529.
[34] J. Wang, M.P. Chatrathi, B.M. Tian, R. Polsky, Anal. Chem. 72 (2000) 2514–2518.
[35] L. Zhang, C.H. Zhang, J.Y. Lian, Biosens. Bioelectron. 24 (2008) 690–695.
[36] J.S. Huang, Y. Liu, H.Q. Hou, T.Y. You, Biosens. Bioelectron. 24 (2008) 632–637.
[37] C.L. Sun, H.H. Lee, J.M. Yang, C.C. Wu, Biosens. Bioelectron. 26 (2011) 3450–3455.
[38] R.A. Poole, F. Kielar, S.L. Richardson, P.A. Stenson, D. Parker, Chem. Commun. (2006) 4084–4086.
[39] A.L. Liu, S.B. Zhang, W. Chen, X.H. Lin, X.H. Xia, Biosens. Bioelectron. 23 (2008) 1488–1495.
[40] Z.H. Sheng, L. Shao, J.J. Chen, W.J. Bao, F.B. Wang, X.H. Xia, ACS Nano 5 (2011) 4350–4358.
[41] L. Zhang, Y. Li, L. Zhang, D.W. Li, D. Karpuzov, Y.T. Long, Int. J. Electrochem. Sci. 6 (2011) 819–829.
[42] U. Chandra, B.E.K. Swamy, O. Gilbert, B.S. Sherigara, Electrochim. Acta 55 (2010) 7166–7174.
[43] S.M. Ghoreishi, M. Behpour, F. Saeidinejad, Anal. Methods 4 (2012) 2447–2453.
[44] F.Y. Zhang, Z.H. Wang, Y.Z. Zhang, Z.X. Zheng, C.M. Wang, Y.L. Du, W.C. Ye, Talanta 93 (2012) 320–325.
[45] X.Q. Lin, Y.X. Li, Electrochim. Acta 51 (2006) 5794–5801.
[46] Y. Wang, L.L. Tong, Sens. Actuators, B 150 (2010) 43–49.